Journal of Power Sources 251 (2014) 319–324

Contents lists available at ScienceDirect

Journal of Power Sources

journal homepage: www.elsevier.com/locate/jpowsour

Short communication

Electrochemical characteristics of ZnSe and its nanostructured composite for rechargeable Li-ion batteries

Hyuk-Tae Kwon, Cheol-Min Park*

School of Advanced Materials and System Engineering, Kumoh National Institute of Technology, Gumi, Gyeongbuk 730-701, Republic of Korea

HIGHLIGHTS

- ZnSe and its nanostructured composite are prepared by simple solid-state synthetic routes.
- The ZnSe and ZnSe/C nanocomposite are tested for their suitability as electrode materials for Li-ion batteries.
- The electrochemical reaction mechanism between ZnSe and Li is demonstrated using ex situ XRD and EXAFS analyses.
- The nanostructured ZnSe/C composite electrode exhibit excellent electrochemical performances.

GRAPHICAL ABSTRACT

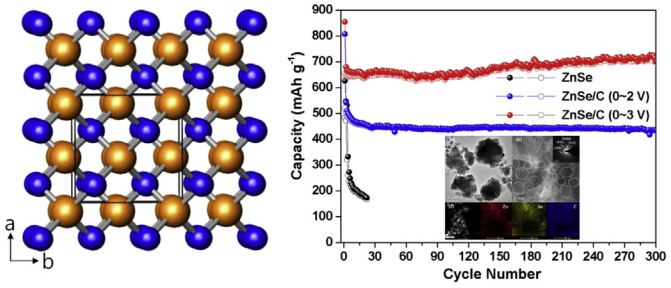

ARTICLE INFO

Article history:
Received 1 October 2013
Received in revised form
14 November 2013
Accepted 16 November 2013
Available online 28 November 2013

Keywords:
Lithium batteries
Anode materials
Nanostructured composite
Zinc selenide

ABSTRACT

Zinc selenide (ZnSe; mineral name: stilleite) and its nanostructured composite (ZnSe/C) are prepared by simple solid-state synthetic routes, and their potential as electrode materials for rechargeable Li-ion batteries is investigated. The reaction mechanism between ZnSe and Li is demonstrated using ex situ X-ray diffraction and extended X-ray absorption fine structure analyses. The X-ray diffraction patterns and high-resolution transmission electron microscopy observations confirm that ZnSe nanocrystallites in ZnSe/C are uniformly distributed within an amorphous carbon matrix. The nanostructured ZnSe/C composite electrode exhibit excellent electrochemical performances such as a high capacity and long cycling behavior of ca. 705 mAh g^{-1} over 300 cycles.

1. Introduction

Since the commercialization of Li-ion batteries by Sony Energytech in 1991, Li-ion batteries have been considered as a promising choice among the representative rechargeable solid-state battery systems such as nickel–cadmium, nickel–metal hydride, and Li-ion. To meet the requirement for longer-lasting electronic mobile devices and hybrid electric vehicles (HEVs), intensive research efforts have been focused on the development of Li-ion batteries with higher capacity and faster rate capability. However, commercial Li-ion batteries, generally composed of a graphite anode and a $LiCoO_2$ cathode, show limited electrochemical performance such as low capacity and slow rate capability. Therefore, higher-capacity alternatives have been actively researched, particularly for anode materials [1–5].

Numerous Li alloy-based materials such as Sn, Si, P, Sb, Mg, Ag, Zn, and Al have been proposed as possible anodes for Li-ion batteries owing to their ability to reversibly react with a large amount

* Corresponding author. Tel.: +82 54 478 7746; fax: +82 54 478 7769.
E-mail address: cmpark@kumoh.ac.kr (C.-M. Park).

0378-7753/$ – see front matter © 2013 Elsevier B.V. All rights reserved.
http://dx.doi.org/10.1016/j.jpowsour.2013.11.033

of Li ions per formula unit [6–20]. Although the Li alloy-based systems have a higher energy density, they generally suffer from poor cycling behavior because of the large volume change that occur during the charge/discharge process. Among the many Li alloying materials available, Zn-based materials have been extensively studied as anode materials in rechargeable Li-ion batteries because Zn has a high theoretical capacity of ca. 410 mAh g^{-1} and can form various Zn–M binary compounds, where M represents ZnSb, ZnP_2, ZnS, and so on [19,21–25]. Additionally, Zn is an abundant, cost-effective, and environmentally friendly element. However, although Zn-based anodes have exhibited enhanced capacity retention, their electrochemical performance is still poor.

Recently, selenium has been used as an electrode material for rechargeable Li batteries [26–31]. Although Se shows a high theoretical capacity (Li_2Se: ca. 679 mAh g^{-1}) when used as the electrode material for Li secondary batteries, it exhibits a low rate capability and poor cycling behavior because of its low electrical conductivity and large volume expansion during cycling. To overcome these disadvantages, the use of a Se/carbon nanocomposites prepared by various synthetic methods have been suggested [29–31]. Recently, carbon nanotube-containing Se/C and SeS_2/C composites [29], and Se/mesoporous carbon composites [30,31] were reported as alternative solutions for enhancement of Se electrode. In these nanocomposites, carbon compensates for the poor electrical conductivity of Se and accommodates its volume expansion during Li insertion/extraction.

ZnSe has been commonly used in the semiconductor industry, specifically in the field of optoelectronic devices such as II–VI light-emitting diodes and blue-green diode lasers, because it is an intrinsic semiconductor with a band gap of approximately 2.7 eV at 298 K. Much effort has been focused on the synthesis of ZnSe nanocrystals or thin solid films by various synthetic methods such as solvothermal and hydrothermal decomposition, metalorganic chemical vapor deposition, and chemical bath deposition methods [32–34].

In this study, in order to overcome the problems faced when Zn or Se is used independently as an electrode material, a ZnSe compound and its nanostructured composite were prepared and tested for their suitability as electrode materials for Li-ion batteries. Further, the reaction mechanism of ZnSe with Li was extensively investigated on the basis of the ex situ X-ray diffraction (XRD) and extended X-ray absorption fine structure (EXAFS) results along with a differential capacity plot (DCP).

2. Experimental

ZnSe was synthesized by the following solid-state synthetic route. Stoichiometric amounts of Zn (Kojundo, 99.9%, average size ca. 150 μm) and Se (Aldrich, 99.5%, average size ca. 100 μm) powders were mixed using high energy mechanical milling (HEMM, Spex-8000) for 1 h and placed into a quartz tube and heated to 900 °C for 5 h under Ar atmosphere at a heating rate of 3 °C min^{-1}. After heating, the furnace was cooled automatically to room temperature. The ZnSe/C nanocomposite was prepared as follows. ZnSe, carbon (Super P), and stainless steel balls (with diameters of 3/8 and 3/16 in.) were placed into a hardened steel vial with a capacity of 80 cm^3 and a ball-to-powder ratio of 20:1. The HEMM process was carried out in an Ar atmosphere for 6 h. Preliminary electrochemical tests revealed that in terms of the electrochemical performance such as initial capacity, initial coulombic efficiency, and cycle performance, the optimum amounts of ZnSe and C were 60 and 40 wt.%, respectively.

The ZnSe sample and its nanostructured composite were characterized using XRD (DMAX2500-PC, Rigaku), high-resolution transmission electron microscopy (HRTEM, FEI F20, operating at 200 kV), and energy-dispersive spectroscopy (EDS) attached to the HRTEM. Ex situ XRD and EXAFS analyses were used to observe the structural changes occurring in the active material of the ZnSe electrode during cycling. The Zn K-edge EXAFS spectra for the ZnSe electrode were recorded at the 8C (Nano XAFS) beamline in a storage ring of 3.0 GeV at the Pohang Light Source (PLS), Korea.

For the electrochemical evaluation of the Zn, Se, and ZnSe and the ZnSe/C composite, test electrodes consisting of the active powder material (70 wt.%), carbon black (Denka, 15 wt.%) as a conducting agent, and polyvinylidene fluoride (PVdF, 15 wt.%) dissolved in *N*-methyl-2-pyrrolidone (NMP) as a binder were fabricated. Samples of each mixture were vacuum-dried at 120 °C for 3 h and pressed (electrode; thickness: ca. 0.045 mm, area: 0.79 cm^2, weight of active material: ca. 2.5 mg). Coin-type electrochemical cells were assembled in an Ar filled glove box using Celgard 2400 as the separator, Li foil as the counter and reference electrodes, and 1 M $LiPF_6$ in ethylene carbonate/diethyl carbonate (EC/DEC, 1:1 by volume, Panax STARLYTE) as the electrolyte. All the cells were tested galvanostatically between 0.0 and 3.0 V (vs. Li/Li^+) at a current density of 100 mA g^{-1} using a Maccor automated tester. Li was inserted into the electrode during discharging and was extracted from the working electrode during charging.

3. Results and discussion

Fig. 1a shows the XRD patterns for the ZnSe sample obtained by a simple solid-state synthesis method. All the peaks corresponded

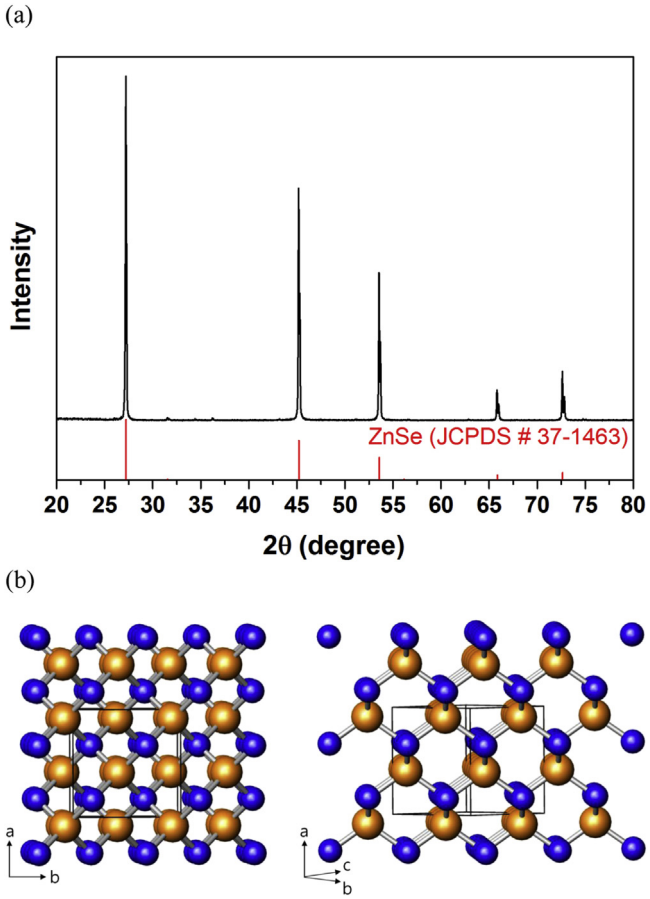

Fig. 1. Characterization of synthesized ZnSe: (a) XRD pattern and (b) crystalline structure (blue: Zn atoms, orange: Se atoms) (For interpretation of the references to colour in this figure legend, the reader is referred to the web version of this article.).

to the ZnSe phase (JCPDS #37-1463) and no other crystalline phases were detected. Fig. 1b shows the crystalline structure of ZnSe (S.G F4-3m, $a = 5.668$ Å), which has a zinc blende structure. The ZnSe compound has an interesting crystalline structure containing hexagonal-type channels along the <01−1> direction that facilitated Li diffusion and accommodation.

The voltage profiles of the Zn, Se, and ZnSe electrodes are shown in Fig. 2a–c, respectively. The first discharge and charge capacities of the Zn electrode were 413 and 206 mAh g^{-1}, respectively, with a poor coulombic efficiency of 49.9% for the first cycle. The poor reversibility of the Zn electrode was caused by the large volume change because of the formation of LiZn, which was associated with the pulverization of the active material and its subsequent electrical isolation from the current collector. The voltage profile of the Se electrode showed small discharge and charge capacities of 109 and 61 mAh g^{-1}, respectively. Considering the theoretical capacity (Li_2Se: 679 mAh g^{-1}) of the Se electrode, the small discharge/charge capacities were attributed to the poor electrical conductivity of Se. The ZnSe electrode showed high reversibility with the first discharge and charge capacities of 627 and 485 mAh g^{-1}, respectively, with a high coulombic efficiency of 77.4%. Considering the theoretical capacity of ZnSe (ca. 557 mAh g^{-1}) and a **solid electrolyte interphase** (SEI) layer formation reaction (ca. 60 mAh g^{-1}) near 0.7 V [35], it can be concluded that the synthesized ZnSe electrode was fully reacted with Li. Although the ZnSe electrode exhibited better electrochemical performance than the Zn and Se electrodes, the capacity retention after the 10th cycle was ca. 40.8% of the first charge capacity. The poor capacity retention of the ZnSe electrode may be caused by the large volume change in the formation of Li_2Se and LiZn phases during the discharge step, followed by pulverization of the active material and its subsequent electrical isolation from the current collector.

In Fig. 3a, the DCP of the first and second cycles of the ZnSe electrode shows several peaks during its discharge and charge. Its ex situ XRD analyses were performed at selected potentials, as indicated in the DCP, and the results are presented in Fig. 3b. When

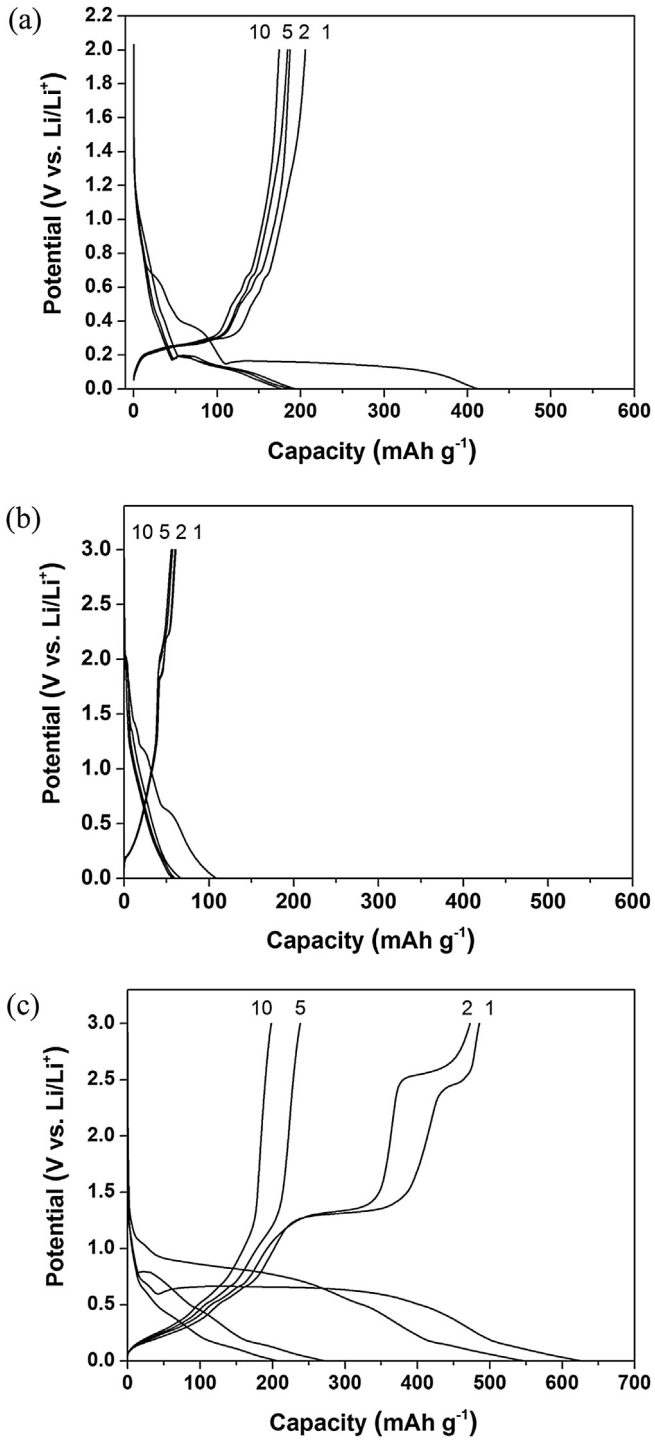

Fig. 2. Voltage profiles of various electrodes: (a) Zn, (b) Se, and (c) ZnSe electrodes.

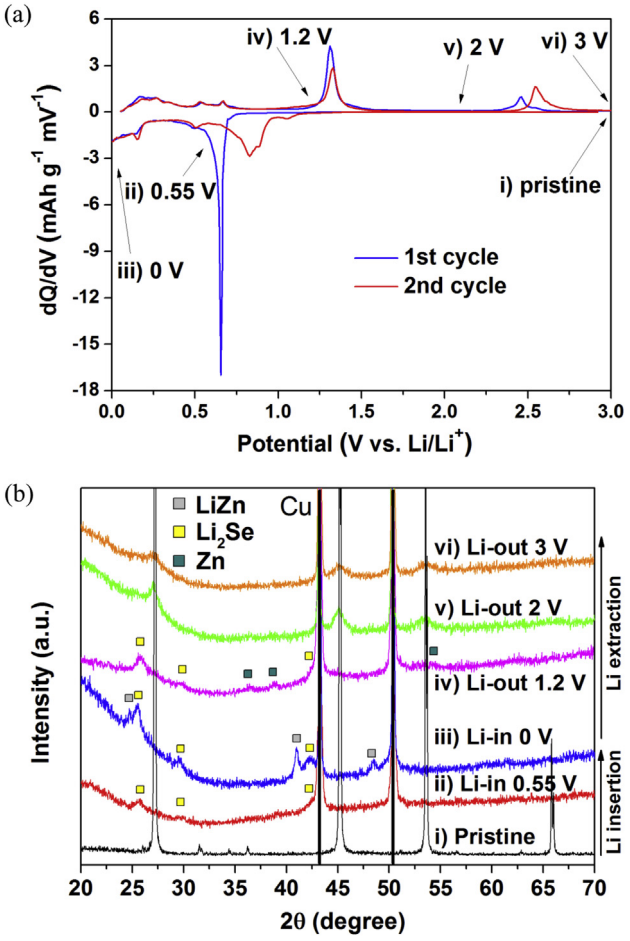

Fig. 3. Electrochemical reaction mechanism between ZnSe and Li: (a) DCP of the first and second cycles; (b) ex situ XRD results of the first cycle for ZnSe [lowercase Roman letters correspond to the potentials indicated in (a)].

the potential was lowered from the open-circuit potential (Fig. 3b-i) to 0.7 V, an extremely small peak was observed, which was caused by the SEI layer formation [35]. When the potential was additionally lowered to the 0.55 V, the Li_2Se phase appeared, as shown in Fig. 3b-ii. In the voltage range between 0.55 and 0 V, various small peaks appeared in the DCP. The reaction potentials of these peaks are in good agreement with those of various Li_xZn alloy phases such as $LiZn_4$, Li_2Zn_5, $LiZn_2$, and Li_2Zn_3. When the electrode was in its fully discharged state of 0.0 V (Fig. 3b-iiii), the XRD pattern showed the presence of LiZn and Li_2Se phases, indicating a full conversion reaction of ZnSe. During the charge step, the LiZn phase disappeared when the potential was increased to 1.2 V and the Zn phase appeared (Fig. 3b-iv). In the further charged state of 2 V (Fig. 3b-v), the Li_2Se and Zn phase was transformed to ZnSe. In the fully charged state of 3 V (Fig. 3b-vi), no structural changes were observed, whereas a broad peak near 2.5 V appeared in the DCP (Fig. 3a).

To confirm the reaction mechanism of the ZnSe electrode more accurately, Zn K-edge EXAFS analyses of the ZnSe electrode were performed and the results are shown in Fig. 4. The main EXAFS peaks in the spectrum for the crystalline ZnSe were associated with the Zn–Zn_{edge} (2.1 Å) and Zn–Zn_{corner} (3.6 Å) bond lengths [36,37]. When the potential was fully discharged to 0 V, the main peaks in the spectrum for ZnSe transformed to 2.35 Å (representing the Zn–Zn interatomic distance in LiZn). In the charged state of 2.0 V, the main EXAFS peaks retransformed to the Zn–Zn_{edge} (2.1 Å) and Zn–Zn_{corner} (3.6 Å) bond lengths of the ZnSe phase. This result demonstrates that the ZnSe phase was recombined during the charge step, results that are consistent with the ex situ XRD results. This recombination reaction phenomenon is quite interesting and similar to those observed with Cu_6Sn_5, ZnP_2, SnSb, Sb_2S_3, and nanosized transition metal oxides [9,23,38–41]. Proof of this recombination reaction phenomenon is also supported by the appearance of the same DCP peaks of the 1st and 2nd cycles shown in Fig. 3a. In the further charged state of 3.0 V, the EXAFS peaks showed no structural variation. The results demonstrate that the broad peak near 2.5 V in the DCP may be related to a subreaction between the electrolyte and surface of the electrode. On the basis of the above ex situ XRD and EXAFS results, the reactions taking place during the first discharge and charge cycle can be expressed as follows:

During discharge:

$$ZnSe \rightarrow Li_2Se + Zn \rightarrow Li_2Se + Li_xZn \rightarrow Li_2Se + LiZn$$

During charge:

$$Li_2Se + LiZn \rightarrow Li_2Se + Li_xZn \rightarrow Li_2Se + Zn \rightarrow ZnSe$$

Although a similar reaction mechanism was suggested by Xue et al. using a thin-film ZnSe electrode [42], our results definitely demonstrate the phase transitions that take place at the ZnSe electrode during Li insertion/extraction. Additionally, the thin-film ZnSe electrode showed very poor electrochemical performances caused by large volume expansion during repeated Li insertion/extraction.

Similar to the Li alloy-based anode in Li-ion battery systems or the S cathode in Li/S battery systems [43–46], the nanocomposites modified with carbon produced by HEMM were suitable for fabricating high-performance electrode materials because this method yielded well-distributed, nanosized metal or alloy crystallites within the carbon matrix. HEMM plastically deforms the particles, which leads to work hardening and fracture of the material upon impact at temperatures >200 °C and pressures on the order of 6 GPa [47]. Upon consideration of the HEMM mechanism, a ZnSe/C composite sample was prepared using HEMM. In Fig. 5, all the XRD peaks of the ZnSe/C composite corresponded to ZnSe peaks, with no other phases detected. The average ZnSe nanocrystallite size in the ZnSe/C nanocomposite estimated using Scherrer's equation was approximately 8.9 nm.

As shown in Fig. 6, the bright-field TEM (Fig. 6a) and HRTEM (Fig. 6b) images combined with selected-area electron diffraction (SAED) patterns indicate the presence of 5–10 nm ZnSe nanocrystallites in the amorphous carbon matrix, results that agree well with the XRD results. The EDS mapping image (Fig. 6c) also indicates that the ZnSe nanocrystallites and carbon were well dispersed within the composite.

Fig. 7 shows the voltage profiles of the ZnSe/C nanocomposite electrode. The initial discharge and charge capacities of the ZnSe/C nanocomposite electrode within the voltage range 0–3.0 V were 855 and 654 mAh g^{-1}, respectively, with a relatively high initial coulombic efficiency of 76%. The initial electrochemical irreversibility of milled amorphous carbon (ca. 200 mAh g^{-1}) in the ZnSe/C nanocomposite indicates the full electrochemical reversibility of the ZnSe in the ZnSe/C nanocomposite electrode [48]. The high reversibility is attributed to the preparation of the ZnSe nanocrystallites within the amorphous carbon matrix, which enhances the electrochemical kinetics and electrical conductivity of the composite material. Additionally, the good electrochemical

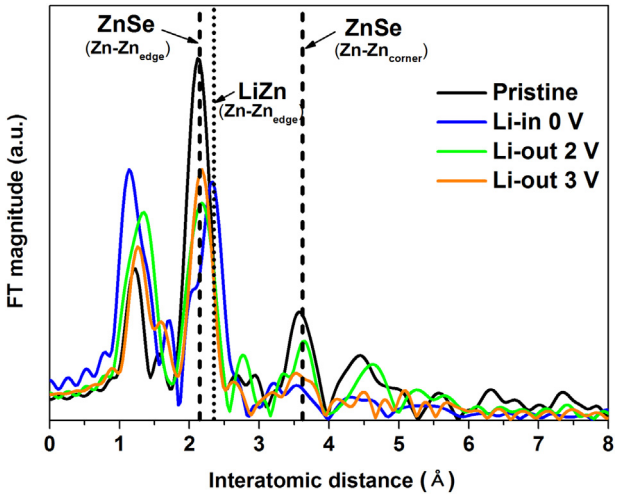

Fig. 4. EXAFS spectra of ZnSe electrode during the first cycle.

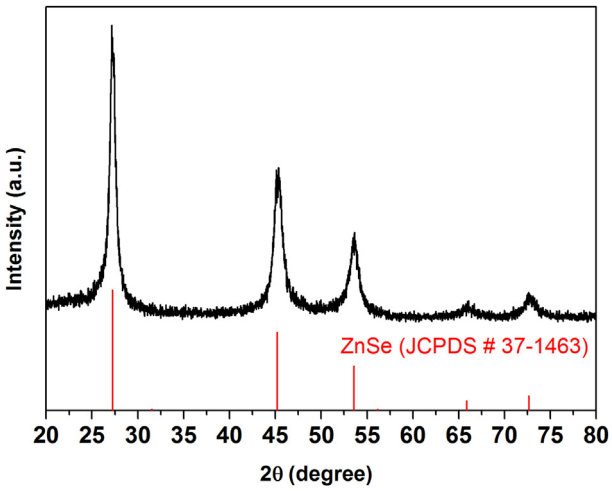

Fig. 5. XRD pattern of ZnSe/C nanocomposite.

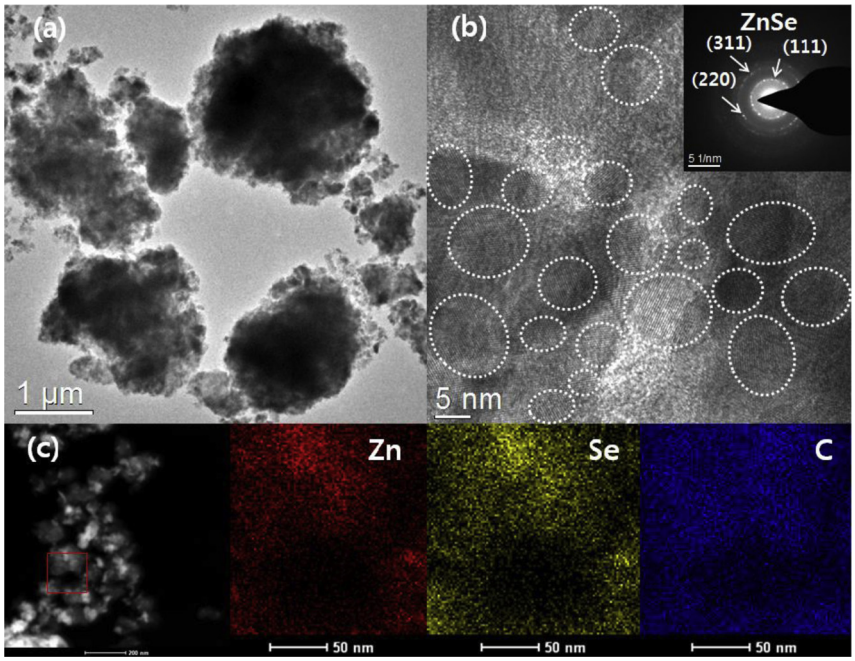

Fig. 6. TEM images of ZnSe/C nanocomposite: (a) bright-field TEM, (b) HRTEM image with corresponding diffraction pattern, and (c) EDS mapping images.

performance can be attributed to the conversion/recombination reactions of the ZnSe during Li insertion/extraction. This is because the nanocrystalline binary intermetallic compounds gradually decreased to 2–3 nm nanocrystallites after a few cycles, and they retained the same size throughout the subsequent discharge/charge cycles by repeatedly dissociating into Li–X and Li–Y phases and then recombining to form the binary intermetallic phase of XY within the composite [49].

The cycle performances were compared for the ZnSe (voltage range: 0–3.0 V) and ZnSe/C nanocomposite (voltage range: 0–2.0 V and 0–3.0 V) electrodes at a current rate of 100 mA g^{-1} (Fig. 8). The cycle performance of the ZnSe electrode was quite poor because of the large volume change that occurred during the formation of the Li_2Se and LiZn phases. The ZnSe/C nanocomposite electrodes showed high electrochemical reversibility and long cycle behaviors compared with those of the ZnSe electrode when it was cycled within the voltage ranges between 0 and 3.0 V (or 2.0 V). The ZnSe/C nanocomposite electrode within the voltage range 0–3.0 V showed a very stable capacity of ca. 705 mAh g^{-1} over 300 cycles. Additionally, in the case of the voltage range between 0 and 2.0 V, the ZnSe/C nanocomposite electrode also showed a very stable capacity retention of ca. 437 mAh g^{-1} over 300 cycles. These excellent cycle performances were attributed to the uniformly distributed active 5–10 nm ZnSe nanocrystallites, the buffering matrix of amorphous carbon, and the conversion/recombination reactions of ZnSe during discharge/charge.

4. Conclusions

The electrochemical conversion/recombination reactions of ZnSe during discharge/charge were demonstrated by conducting ex situ XRD and EXAFS analyses on the basis of the DCP results for the ZnSe electrode. A ZnSe/C nanocomposite composed of 5–10 nm ZnSe nanocrystallites distributed uniformly within a carbon matrix

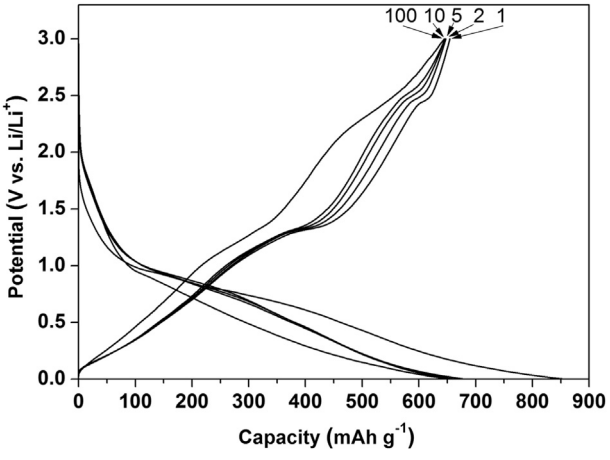

Fig. 7. Voltage profile of ZnSe/C nanocomposite electrode within voltage range 0–3.0 V.

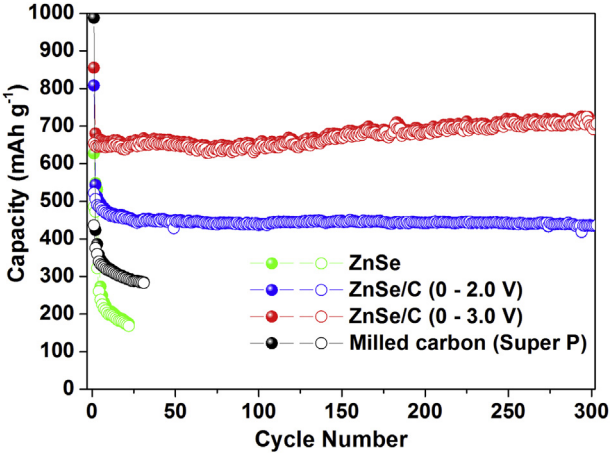

Fig. 8. Comparison of cycle performances of pristine ZnSe (voltage range: 0–3.0 V), ZnSe/C nanocomposite (voltage range: 0–2.0 V), and ZnSe nanocomposite (voltage range: 0–3.0 V) electrodes.

was prepared and tested to examine its suitability as an electrode material for Li secondary batteries. The ZnSe/C nanocomposite electrode exhibited excellent electrochemical performances such as a high capacity and long cycling behavior of ca. 705 mAh g^{-1} over 300 cycles (voltage range: 0–3.0 V).

Acknowledgments

This research was supported by the Basic Science Research Program through the National Research Foundation of Korea (NRF) funded by the Ministry of education, Science and Technology (NRF-2011-0013624).

References

[1] G.-A. Nazri, G. Pistoia, Lithium Batteries: Science and Technology, Kluwer Academic/Plenum, Boston, 2004.
[2] C.-M. Park, J.-H. Kim, H. Kim, H.-J. Sohn, Chem. Soc. Rev. 39 (2010) 3115–3141.
[3] M. Winter, J.O. Besenhard, M.E. Spahr, P. Novak, Adv. Mater 10 (1998) 725–763.
[4] R.A. Huggins, J. Power Sources 81–82 (1999) 13–19.
[5] D. Larcher, S. Beattie, M. Morcrette, K. Edstrom, J.-C. Jumas, J.-M. Tarascon, J. Mater. Chem. 17 (2007) 3759–3772.
[6] Y. Idota, T. Kubota, A. Matsufuji, Y. Maekawa, T. Miyasaka, Science 276 (1997) 1395–1397.
[7] C.J. Wen, R.A. Huggins, J. Solid-State Chem 37 (1981) 271–278.
[8] C.-M. Park, Y. Hwa, N.-E. Sung, H.-J. Sohn, J. Mater. Chem. 20 (2010) 1097–1102.
[9] S.D. Beattie, D. Larcher, M. Morcrette, B. Simon, J.M. Tarascon, J. Electrochem. Soc. 155 (2008) A158–A163.
[10] M. Yoshio, H.Y. Wang, K. Fukuda, T. Umeno, N. Dimov, Z. Ogumi, J. Electrochem. Soc. 149 (2002) A1598–A1603.
[11] J. Graetz, C.C. Ahn, R. Yazami, B. Fultz, J. Electrochem. Soc. 151 (2004) A698–A702.
[12] I.-S. Kim, P.N. Kumta, J. Power Sources 136 (2004) 145–149.
[13] J. Hassoun, G. Derrien, S. Panero, B. Scrosati, Adv. Mater. 20 (2008) 3169–3175.
[14] M.-S. Park, S.A. Needham, G.-X. Wang, Y.-M. Kang, J.-S. Park, S.-X. Dou, H.-K. Liu, Chem. Mater. 19 (2007) 2406–2410.
[15] C.-M. Park, H.-J. Sohn, Adv. Mater. 19 (2007) 2465–2471.
[16] C.-M. Park, H.-J. Sohn, Chem. Mater. 20 (2008) 3169–3173.
[17] C.K. Chan, H. Peng, G. Liu, K. McIlwrath, X.F. Zhang, R.A. Huggins, Y. Cui, Nature Nanotech. 3 (2008) 31.
[18] C.-M. Park, H. Jung, H.-J. Sohn, Electrochem. Solid State Lett. 12 (2009) A171–A175.
[19] Y. Hwa, J.H. Sung, B. Wang, C.-M. Park, H.-J. Sohn, J. Mater. Chem. 22 (2012) 12767–12773.
[20] G.-J. Jeong, Y.U. Kim, H.-J. Sohn, T. Kang, J. Power Sources 101 (2001) 201–205.
[21] C.-M. Park, H.-J. Sohn, Adv. Mater. 22 (2010) 47–52.
[22] J. Wang, G. Wang, L. Yang, S.H. Ng, H. Liu, J. Solid State Electrochem. 10 (2006) 250–254.
[23] C.-M. Park, H.-J. Sohn, Chem. Mater. 20 (2008) 6319–6324.
[24] M.-P. Bichat, J.-L. Pascal, F. Gillot, F. Favier, Chem. Mater. 17 (2005) 6761–6771.
[25] M.-P. Bichat, L. Monconduit, J.-L. Pascal, F. Favier, Ionics 11 (2005) 66–75.
[26] M.Z. Xue, J. Yao, S.C. Cheng, Z.W. Fu, J. Electrochem. Soc. 153 (2006) A270.
[27] M.Z. Xue, Z.W. Fu, Electrochem. Commun. 8 (2006) 1855.
[28] L. Liu, Y. Hou, X. Wu, S. Xiao, Z. Chang, Y. Yang, Y. Wu, Chem. Commun. 49 (2013) 11515–11517.
[29] A. Abouimrane, D. Dambournet, K.W. Chapman, P.J. Chupas, W. Weng, K. Amine, J. Am. Chem. Soc. 134 (2012) 4505–4508.
[30] C.-P. Yang, S. Xin, Y.-X. Yin, H. Ye, J. Zhang, Y.-G. Guo, Angew. Chem. Int. Ed. 52 (2013) 8363–8367.
[31] C. Luo, Y. Xu, Y. Zhu, Y. Liu, S. Zheng, Y. Liu, A. Langrock, C. Wang, ACS Nano 7 (2013) 8003–8010.
[32] C. Wang, W.X. Zhang, X.F. Qian, X.M. Zhang, Y. Xie, Y. Qian, Mater. Chem. Phys. 60 (1999) 99–102.
[33] B. Su, K.L. Choy, Thin Solid Films 361 (2000) 102–106.
[34] Y. Noda, Y. Ishikawa, M. Yamabe, Y. Hara, Appl. Sur. Sci. 113/114 (1997) 28–32.
[35] P.B. Balbuena, Y. Wang, Lithium-ion Batteries: Solid–electrolyte Interphase, Imperial College Press, 2004.
[36] D. Diop, R. Grisenti, Physica B 208/209 (1995) 164–166.
[37] R.G. Valeev, A.N. Deev, F.Z. Gilmutdinov, S.G. Bystrov, O.I. Pivovarova, E.A. Romanov, V.V. Kriventsov, M.R. Sharafutdinov, A.A. Eliseev, J. Struct. Chem. 49 (2008) S124–S128.
[38] K.D. Kepler, J.T. Vaughey, M.M. Thackeray, Electrochem. Solid-State Lett. 2 (1999) 307–309.
[39] J. Yang, M. Winter, J.O. Besenhard, Solid State Ionics 90 (1996) 281–287.
[40] C.-M. Park, K.-J. Jeon, Chem. Commun. 47 (2011) 2122–2124.
[41] P. Poizot, S. Laruelle, S. Grugeon, L. Dupont, J.-M. Tarascon, Nature 407 (2000) 496–499.
[42] M.-Z. Xue, Z.-Wen Fu, Electrochim. Acta 52 (2006) 988–995.
[43] W. Zheng, Y.W. Liu, X.G. Hu, C.F. Zhang, Electrochim. Acta 51 (2006) 1330–1335.
[44] C. Liang, N.J. Dudney, J.Y. Howe, Chem. Mater. 21 (2009) 4724–4730.
[45] X. Ji, K.T. Lee, L.F. Nazar, Nature Mater. 8 (2009) 500–506.
[46] A. Manthiram, Y. Fu, Y.-S. Su, Acc. Chem. Res. 46 (2013) 1125–1134.
[47] C. Suryanarayana, Prog. Mater. Sci. 46 (2001) 1–184.
[48] J.H. Sung, C.-M. Park, Mater. Lett. 98 (2013) 15–18.
[49] C.-M. Park, H.-J. Sohn, Electrochim. Acta 54 (2009) 6367–6373.